



Real-time monitoring of extracellular pH using a pH-potentiometric sensing SECM dual-microelectrode

Ranran Song¹ · Qiang Xiong¹ · Tao Wu¹ · Xin Ning¹ · Fan Zhang¹ · Qingjiang Wang¹ · Pingang He¹

Received: 8 February 2020 / Revised: 25 March 2020 / Accepted: 27 March 2020 / Published online: 3 May 2020
© Springer-Verlag GmbH Germany, part of Springer Nature 2020

Abstract

Extracellular pH can indicate the variation in organelle function and cell state. It is important to measure extracellular pH (pHe) with a controllable distance. In this work, a potentiometric SECM dual-microelectrode was developed to monitor the pHe of MCF-7 cells under electrical stimulation. The distance between the dual-microelectrode and the cells was determined first with a gold microelectrode by recording the approaching curve, and the pH was determined using an open-circuit potential (OCP) technique with a polyaniline-modified Pt microelectrode. The pH microelectrode showed a response slope of 53.0 ± 0.4 mV/pH and good reversibility from pH 4 to pH 8, fast response within 10 s, and a potential drift of 1.13% for 3 h, and thus was employed to monitor the pHe of stimulated cells. The value of pHe decreased with the decrease in the distance to cells, likely due to the release of H^+ . With an increase in the stimulation potential or time, the pHe value decreased, as the cell membrane became more permeable, which was verified by fluorescence staining of calcein-AM/PI (propidium iodide). Based on these results, this method can be widely applied for determining the species released by biosystems at a controllable position.

Keywords Scanning electrochemical microscopy · Dual-microelectrode · Extracellular pH · Potentiometric sensing · Real-time monitoring

Introduction

Cells are the basic structural and functional units of organisms, and the main site of metabolism [1]. Cell survival largely depends on the balance of intracellular pH (pHi), which can regulate metabolic pathways such as signaling, defense, immune function, and apoptosis [2, 3]. To maintain this balance, numerous protons are transported to the extracellular environment by Na^+/H^+ exchanger (NHE-1), single carboxylic acid

transport (MCT), and V-type ATPase, resulting in a decrease in extracellular pH (pHe) [4–8]. In other words, the changes in pHe are attributed to intracellular metabolism. Thus, an abnormal pHe could indicate abnormal organelle function, which is associated with many diseases. For example, the pHe of normal cells (7.2–7.4) is higher than that of cancer cells (6.2–6.8) [9]. The low pHe of cancer cells promotes the degradation of the extracellular matrix in order to enhance cell invasion [10] and reduce adhesion [11]. pHe also has an effect on the uptake of anticancer drugs and response to therapy [12]. Therefore, the development of techniques for measuring pHe in a continuous manner is essential.

Glass electrodes have been widely used in pH detection under various working conditions for their advantages of high sensitivity, good long-term stability, high measurement accuracy, and good ion selectivity [13]. However, glass electrodes are filled with liquid, and can only be used to measure large-volume solutions, so they are not conducive to miniaturization [13]. On the other hand, miniaturized electrodes are essential, because the measurement of extracellular pH is within the microregion. Fluorescence [14–17] and surface-enhanced Raman spectroscopy [18–21] have also been employed for

Ranran Song and Qiang Xiong contributed equally to this work.

Electronic supplementary material The online version of this article (<https://doi.org/10.1007/s00216-020-02625-5>) contains supplementary material, which is available to authorized users.

- ✉ Fan Zhang
fzhang@chem.ecnu.edu.cn
- ✉ Qingjiang Wang
qjwang@chem.ecnu.edu.cn

¹ School of Chemistry and Molecular Engineering, East China Normal University, 500 Dongchuan Road, Shanghai 200241, China

pHe monitoring. Fluorescence spectroscopy has high spatial and temporal sensitivity, and has been widely used in monitoring pHe of living cells. However, it requires modification via a fluorescent probe sensitive to pH variation on the surface of cells [17]. The photobleaching and quenching of a fluorescent probe might affect the accuracy of pH detection [22]. Surface-enhanced Raman spectroscopy also introduces signal molecules into the system for the detection of pHe, which may change the physiological state of cells [1]. Ion-sensitive field-effect transistors [23], positron emission tomography [24], and magnetic resonance imaging [25, 26] have also been used to measure pHe, but these methods cannot monitor pHe changes in real time with the variation in cellular state at a controllable position.

Scanning electrochemical microscopy (SECM) is capable of monitoring the concentration distribution near various target objects with voltammetric or potentiometric probes [27–29] at a controllable distance from the substrate. In SECM, the potentiometric mode is widely used to image the concentration distribution of targets such as bacterial biofilm, dental caries, and steel corrosion [30–33]. However, to the best of our knowledge, there are few reports of its use for measuring pHe. Horrocks et al. first proposed using an antimony microdisk for positioning and pH profiling from a glass capillary filled with gelatinized yeast cells [34]. However, antimony electrodes continuously adsorb oxides, and the thicker oxide film affects the accuracy of the pH determination. This is a significant factor restricting the wide and accurate application of Sb pH electrodes [35]. Munteanu et al. designed a voltammetric pH microsensor using a syringaldazine-modified carbon fiber microelectrode 37 μm in diameter as the SECM tip to monitor the pHe of mammalian cells under different oxygen content, achieving high spatial resolution [36]. However, monitoring pHe with a voltammetric pH sensor in a continuous manner is difficult, and as a result, important dynamic information can be missed. Potentiometric sensors with ion-selective electrodes have been used for ion determination, such as Na^+ , K^+ , Cl^- and H^+ [37–39]. For pH sensing, polyaniline is commonly used as a modification material on electrodes and has been used in much research [13, 40, 41].

Here, real-time monitoring of extracellular pH under electrical stimulation was carried out using a potentiometric SECM with a dual-microelectrode probe in a continuous manner. The dual-microelectrode consisted of an Au microelectrode and a polyaniline-modified (PANI) Pt microelectrode 25 μm in diameter, which were used to determine the distance to cells and monitor the pHe in real time, respectively. The open-circuit potential (OCP) responses were continuously collected at variable distances and under variable stimulation potentials and time to investigate the difference in pHe values, thus providing a new means for the real-time

determination of species released by cells exposed to external stimulus conditions.

Experimental section

Chemicals and materials

Ferrocene methanol (FcMeOH) was purchased from Sigma-Aldrich (USA). Aniline was obtained from Sinopharm Chemical Reagent Co., LTD. Calcein-AM/propidium iodide (PI) suitable for fluorescence was obtained from Dojindo Chemical Technology Co., Ltd. (Shanghai, China). Dulbecco's modified Eagle's medium (DMEM), penicillin/streptomycin (P/S), trypsin/EDTA solution, and fetal bovine serum (FBS) solution were purchased from Thermo Fisher (Waltham, MA, USA). Borosilicate glass capillary (1.0 mm OD \times 0.75 mm ID) tubing was obtained from Sutter Instrument Company (USA). Platinum wire (d = 25 μm) and gold wire (d = 25 μm) were purchased from Alfa Aesar (USA). ITO (indium tin oxide 4 cm \times 5 cm, sheet resistance $<7 \Omega/\text{sq}$) glass was provided by Zhuhai Kaivo Optoelectronic Technology Co. Ltd. (China). Phosphate-buffered saline (PBS, 0.01 M, pH = 7.40) solution was prepared with deionized water (DI, $18.2 \text{ M}\Omega \cdot \text{cm}^{-1}$). The human breast cancer cell line (MCF-7) was obtained from the Chinese Academy of Sciences (Shanghai, China).

Instruments

MCF-7 cells were cultured in a humidified incubator (NuAire, USA). Scanning electron microscopy (SEM) characterization of the dual-microelectrode was performed on a Hitachi S-4800 scanning electron microscope (Tokyo, Japan). OCP detection was carried out using a CHI 920C scanning electrochemical microscope (CH Instruments Co., Shanghai, China). MCF-7 cells were electrically stimulated using a CHI 830B electrochemical workstation (CH Instruments Co., Shanghai, China). Drawing borosilicate glass capillary tubes was performed on a P-2000 laser puller (Sutter Instrument Company, USA). Live/dead staining images were obtained with an Olympus IX51 inverted fluorescence microscope (Olympus Corporation, Japan).

Fabrication of the SECM dual-microelectrode

A borosilicate glass capillary tube (OD 1.0 mm, ID 0.75 mm) was first pulled with a pipette puller (Sutter Instruments, Novato, CA, USA), obtaining a pipette with an inner diameter of 60–100 μm (RG < 5) by polishing it on sandpaper. The long platinum and polyimide-coated gold wires with 25- μm diameter were then inserted into the pipette, followed by connection to the respective copper wire by conductive silver

epoxy. With the help of a microscope, they were carefully pulled back to close the glass tube, an appropriate amount of epoxy resin was injected for encapsulation, and the pipette was heated at 120 °C for 1 h to solidify the epoxy resin. To expose the platinum and gold wires, the pipette surface was then polished with sandpaper, finally obtaining the SECM dual-microelectrode consisting of platinum and Au wires. The dual-microelectrode was polished with sandpaper before each experiment. The size was determined by cyclic voltammetry scanning, which was performed in 0.1 M KCl aqueous solution containing 1 mM ferrocene methanol. SEM was used to verify the coating of polyaniline on the surface of the Pt microelectrode in the dual-microelectrode.

Fabrication of the polyaniline-modified Pt microelectrode

Prior to the electropolymerization of aniline, the platinum microelectrode was electrochemically cleaned in 0.5 M H₂SO₄ by cyclic voltammetric in a potential range of −0.25 to 1.55 V. Electropolymerization was then performed in 1 M HCl containing 0.1 M aniline between −0.1 V and 0.9 V (vs. an Ag/AgCl-saturated KCl reference electrode). Polymerization in HCl supporting electrolyte generated smooth morphology of polyaniline [13, 42]. To achieve the best potentiometric response of pH, the number of cycles and the cyclic voltammetry sweep rate for electropolymerization were optimized. The performance of the obtained polyaniline-modified Pt microelectrode was then investigated by OCP.

Cell culture

MCF-7 cells were cultured in DMEM supplemented with 10% FBS and 100 µg/mL P/S at 37 °C in a humidified atmosphere containing 5% CO₂. After reaching 80% confluence, cells were detached with 0.25% trypsin/EDTA. The cells were then resuspended in culture medium after removal of the trypsin/EDTA solution. The concentration of cells was determined by counting with trypan blue staining, followed by seeding on ITO glass with an area of 0.28 cm² at a density of 20,000 cells/cm² for further investigation.

Real-time monitoring of pHe by the SECM dual-microelectrode

The distance between the tip and substrate was first determined by recording approach curves over the cells with the Au microelectrode at 0.450 V in 0.01 M PBS containing 1 mM FcMeOH. When the current decreased to 75% of the initial value, the dual-microelectrode was stopped. After replacing 0.01 M PBS containing 1 mM FcMeOH with 0.01 M PBS, the dual-microelectrode was elevated a certain distance. The OCP response was measured with an Ag/AgCl (saturated

KCl) reference electrode in PBS solution, to avoid fouling of the dual-microelectrode.

After culturing for 24 h, MCF-7 cells were stimulated at a constant potential (0, 0.3, 0.6, 0.9, and 1.2 V) with a three-electrode system in PBS (0.01 M, pH = 7.40) solution [43]. The ITO substrate, Ag/AgCl (saturated KCl) electrode and Pt wire were used as the working electrode, reference electrode and counter electrode, respectively. OCP detection was then performed to investigate the changes in pHe, which were calculated by the change in potential divided by the slope of the pH microelectrode response.

Cell viability was further evaluated by staining with calcein AM (2 µM) and PI (4.5 µM) for 20 min. After washing with PBS solution (10 mM, pH = 7.40) three times, the cells were observed using an Olympus IX51 inverted fluorescence microscope with a fluorescence detector and a 10 × objective.

Results and discussion

Characterization of the SECM dual-microelectrode

The size of the fabricated SECM dual-microelectrode was characterized by cyclic voltammetry and SEM. As shown in Fig. S1 (see [Electronic Supplementary Material](#), ESM), the CV curves of both Au and platinum microelectrodes displayed a sigmoidal shape. According to the equation $I_{ss} = 4nFDc_{eff}$, where I_{ss} is the steady-state current (A), n is the number of electrons involved in the reduction of FcMeOH, F is the Faraday constant (96,485 C/mol), D is the diffusion coefficient of FcMeOH (7.8×10^{-6} cm²/s) [44], C is the concentration of FcMeOH (1.0 mM), and r_{eff} is the radius of the microelectrode (cm), r_{eff} of the Au and Pt microelectrodes was calculated as 12.62 µm with a detected current of 3.8 nA. The size of the microelectrode was further verified by SEM (see ESM Fig. S3), which clearly displayed both microelectrodes with diameter of 25.0 µm. The aniline electropolymerization curve is shown in ESM Fig. S2. The peak at 0.25 V corresponds to the formation of radical cations, and the peak at 0.85 V is likely caused by the conversion from an emeraldine to a pernigraniline structure, which indicates regular growth of the polymer film. Two reduction peaks at 0.55 V and 0.1 V appeared due to the conversion from pernigraniline to emeraldine and from emeraldine to leucoemeraldine, respectively [45]. The SEM image in Fig. S3B (see ESM) also displays a uniform layer on the Pt microelectrode, indicating that the surface was modified with polyaniline. The performance of the polyaniline-modified Pt microelectrode was further investigated by OCP. A series of standard buffer solution values with pH ranging from 4.00 to 8.00, covering the full pH variation of the extracellular environment, were sequentially measured, followed by detection in reverse order. Response slopes of 52.6 mV/pH and 53.2 mV/pH were obtained,

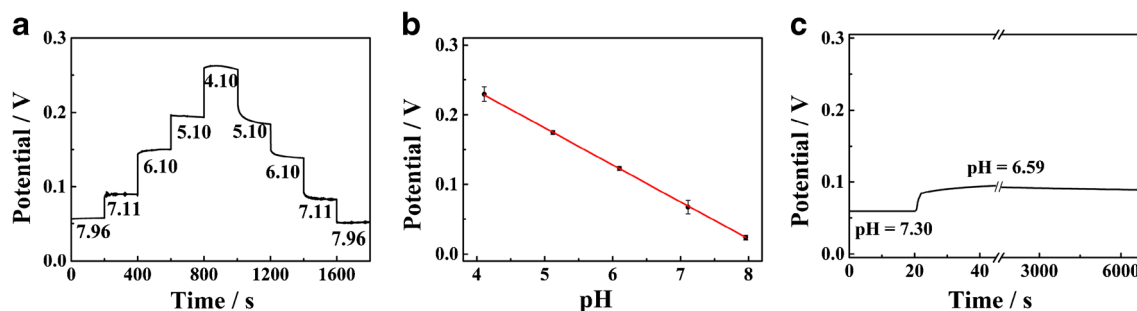


Fig. 1 Potentiometric response characteristics of the pH microelectrode: (a) OCP responses of standard buffer solution in a pH range of 4–8. (b) Deduced calibration curve of the pH microelectrode. (c) Time-dependent

OCP responses of the pH microelectrode to an injection of 0.1 mol/L HCl into PBS solution at pH 7.30 and the continuous monitoring of OCP values at pH 6.59

respectively (Fig. 1a), indicating good reversibility of the pH microelectrode. Figure 1b shows the deduced linear correlation between the potential and pH value, with a slope of 53.0 ± 0.4 mV/pH ($R^2 = 0.9995$), which displays a sub-Nernstian behavior. Six dual-microelectrodes were randomly selected for the detection, and the relative standard deviation (RSD) was 0.76% (see ESM Table S1), showing good reproducibility. From Fig. 1c, it can be observed that the pH microelectrode exhibits a nearly instantaneous response to the pH change from 7.30 to 6.59, yielding 90% of the steady-state signal within the first 5 s, and a completely stable response within 20 s. According to IUPAC criteria, electrode response time is defined as the time when electrode potential reaches 95% of the stable value [46]. Therefore, we determined that 10 s was the response time of the polyaniline-modified electrode. When the measurement was performed continuously in the solution at pH 6.59, the potential drifted only 0.6 mV (1.13%) after 3 h (Fig. 1c), revealing satisfactory stability.

Real-time monitoring of pH at different distances from the cells

In order to determine the change in pHe values with the variation in the cellular state, electrical stimulation was applied to the MCF-7 cells, followed by real-time monitoring of pHe by OCP. Electrical stimulation has been widely used in nerve repair, tissue regeneration, and the induction of apoptosis and differentiation, but has only focused on changes in tissues and cells [47–49]. Few researchers have explored the effect of electrical stimulation on the microenvironment around cells [43], and no reported studies have investigated the variation in extracellular pH under electrical stimulation. When cells are stimulated, H^+ released by cells will spread into the bulk solution from the surface, resulting in different pHe at different distances. Therefore, distance determination is important for investigating the pH gradient around the cells, which was performed by recording the approach curves with the Au microelectrode. In the SECM negative feedback mode, current approximation is typically used to determine the distance between the probe and the substrate [30, 36, 50]. Although the

absolute distance cannot be measured by this method, we can use this method to lower the dual-microelectrode probe to a certain position as the relative position between the probe and the cell. As shown in Fig. S4 (see ESM), negative feedback was clearly observed when the dual-microelectrode approached the cell, compared with the ITO surface. As the current decreased to 75% of the initial value, the dual-microelectrode stopped so as not to damage the cell. The dual-microelectrode was then elevated, followed by OCP determination. The OCP responses at different distances from the cells were extracted 10 s after the stimulation, and the pHe values were calculated according to the equation $pH = 7.35 - \Delta E/0.053$, where 7.35 is the pH value of the bulk solution detected by the pH meter, ΔE is the difference between the OCP value detected at a certain position and the value of the bulk solution, and 0.053 V/pH is the response slope. As shown in Fig. 2, pHe values at 10,000 μm and 10 μm without stimulation were 7.35 (black curve) and 7.17 (red curve), respectively. The pHe at 10,000 μm was the same

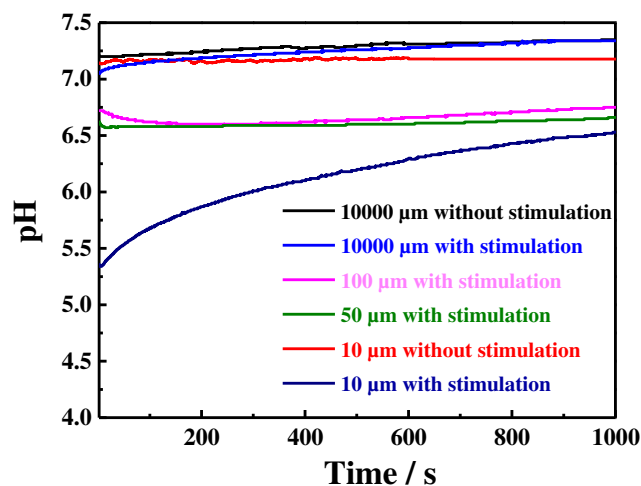
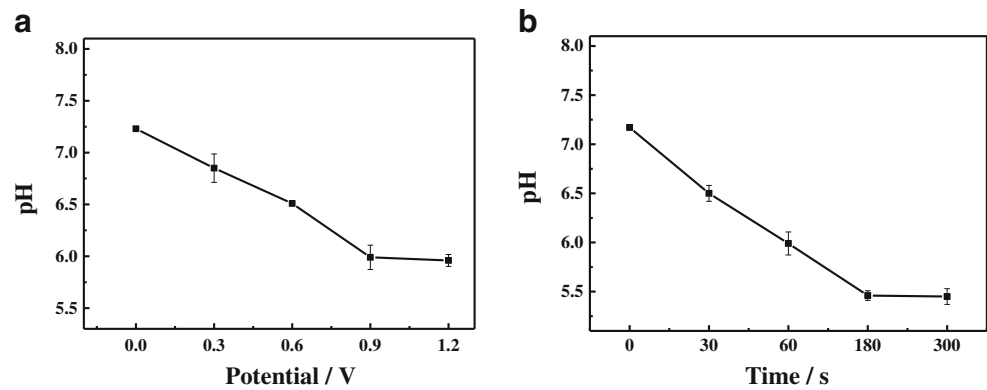


Fig. 2 Variation in pHe over time at different positions between the dual-microelectrode and the cells: 10000 μm with (blue curve) and without stimulation (black curve), 100 μm with stimulation (magenta curve), 50 μm with stimulation (green curve), and 10 μm with (navy curve) and without stimulation (red curve). The electrical stimulation was applied at 0.6 V for 60 s

Fig. 3 Values of pHe at 50 μm with (a) different stimulation potential for 60 s and (b) different stimulation time at 0.9 V



as the pH value of the bulk solution, and the lower pHe value was obtained near the cells, which is consistent with the fact that the pHe of cancer cells is more acidic [9]. In addition, the pHe values at these two positions were nearly constant over time. After the application of electrical stimulation at 0.6 V for 60 s, the pHe at 10,000 μm (blue curve) was essentially unchanged compared with the value before stimulation. When the distance decreased to 100 μm , the pHe value decreased significantly (magenta curve), and further decreases were obtained at 50 μm (green curve) and 10 μm (navy curve), which revealed the release of H^+ by the cells, followed by diffusion to the bulk solution. The pHe values at 100 μm and 50 μm remained nearly unchanged with the prolongation of time once reaching diffusion equilibrium. However, the pHe value at 10 μm increased significantly over time, because of the smaller volume and smaller buffer capacity of the buffer solution. In addition, OCP signals were collected at 10 μm from the ITO substrate before and after stimulation at 0.9 V for 300 s (ESM Fig. S5), showing almost no change, and thus verifying that ITO had no effect on the pH of the solution.

Determination of pHe under variable stimulation conditions

To further investigate the influence of electrical stimulation on pHe, MCF-7 cells were stimulated at different potentials or for different durations. As shown in Fig. 3, pHe gradually decreased with the increase in stimulation potential or stimulation time, indicating that more H^+ were released at a higher potential or longer time period. This is likely due to the change in cell membrane permeability caused by the stimulation. For verification, cell viability was evaluated by fluorescence staining of calcein-AM/PI. Calcein-AM can pass through the cell membrane, and the AM group is then removed by esterase action in living cells, thus producing strong green fluorescence by calcein. Hence, living cells are represented by green fluorescence. On the other hand, PI can enter the cells with damaged membranes, displaying red fluorescence. Clearly, the increased stimulation potential (Fig. 4a–e) and time (Fig. 4f–j) both led to decreased cell viability and thus enhanced membrane permeability. Therefore, more H^+ were released, causing a decrease in pHe.

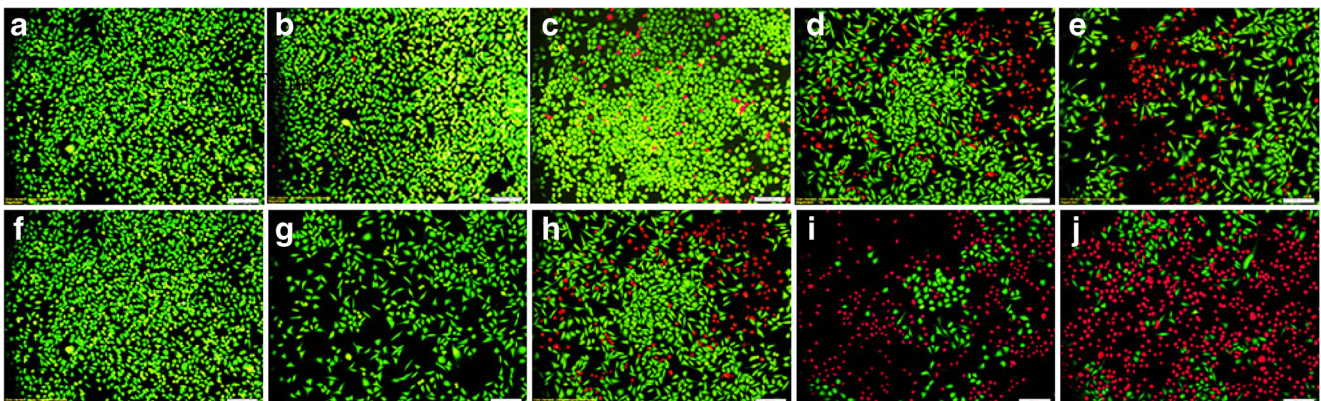


Fig. 4 Evaluation of cell viability under electrical stimulation at (a) 0 V, (b) 0.3 V, (c) 0.6 V, (d) 0.9 V and (e) 1.2 V for 60 s, and at 0.9 V for (f) 0 s, (g) 30 s, (h) 60 s, (i) 180 s and (j) 300 s. The scale bars are 100 μm

Conclusions

In summary, potentiometric monitoring of extracellular pH with an SECM dual-microelectrode, consisting of an Au microelectrode and polyaniline-modified Pt microelectrode, was developed to monitor the pHe of MCF-7 cells under electrical stimulation in real time. An Au microelectrode was used to determine the distance between the dual-microelectrode and the cells through the approaching curve, and the OCP responses under stimulation were then monitored in real time by a polyaniline-modified Pt microelectrode. This pH microelectrode demonstrated satisfactory linear response, with a slope of 53.0 ± 0.4 mV/pH and reversibility in a pH range of 4–8, along with a fast response within 10 s. Stimulation caused the release of H^+ from the cells, and a lower pHe value was obtained at a shorter distance from the cells. Decreased pHe values were detected by increasing the stimulation potential or time, which enhanced the cell membrane permeability, verified by fluorescence staining. It was possible to determine pHe under electrical stimulation with an SECM dual-microelectrode in a continuous manner by fixing the dual-microelectrode probe. Thus, we have a better understanding of the effects of electrical stimulation on cells. This method shows great potential for application to the real-time detection of species released by cells or other bio-targets.

Acknowledgments This work was financially supported by the National Natural Science Foundation of China (Grant No. 21575042).

Compliance with ethical standards

This work does not contain any studies with human participants or animals performed by any of the authors.

Conflicts of interest The authors declare that they have no conflict of interest.

References

- Cialla-May D, Zheng X-S, Weber K, Popp J. Recent progress in surface-enhanced Raman spectroscopy for biological and biomedical applications: from cells to clinics. *Chem Soc Rev*. 2017;46(13):3945–61.
- Liu L, Dou C-X, Liu J-W, Wang X-N, Ying Z-M, Jiang J-H. Cell surface-anchored DNA Nanomachine for dynamically tunable sensing and imaging of extracellular pH. *Anal Chem*. 2018;90(19):11198–202.
- Bishnoi SW, Rozell CJ, Levin CS, Gheith MK, Johnson BR, Johnson DH, et al. All-optical nanoscale pH meter. *Nano Lett*. 2006;6(8):1687–92.
- Cheng P-C, Lin H-Y, Chen Y-S, Cheng R-C, Su H-C, Huang R-C. The Na^+/H^+ -exchanger NHE1 regulates extra- and intracellular pH and nimodipine-sensitive $[Ca^{2+}]_i$ in the suprachiasmatic nucleus. *Sci Rep*. 2019;9(1):1–18.
- Yang OC, Loh S-H. Acidic stress triggers sodium-coupled bicarbonate transport and promotes survival in A375 human melanoma cells. *Sci Rep*. 2019;9(1):1–12.
- Sarangarajan R, Shumaker H, Soleimani M, Le Poole C, Boissy RE. Molecular and functional characterization of sodium–hydrogen exchanger in skin as well as cultured keratinocytes and melanocytes. *Biochimica et Biophysica Acta (BBA)-Biomembranes*. 2001;1511(1):181–92.
- Nishisho T, Hata K, Nakanishi M, Morita Y, Sun-Wada G-H, Wada Y, et al. The $\alpha 3$ isoform vacuolar type H^+ -ATPase promotes distant metastasis in the mouse B16 melanoma cells. *Mol Cancer Res*. 2011;9(7):845–55.
- Wahl ML, Owen JA, Burd R, Herlands RA, Nogami SS, Rodeck U, et al. Regulation of intracellular pH in human melanoma: potential therapeutic implications 1 supported by NIH Grant P01 CA56690 (to MLW, RB, CSO, DBL); Grant R25CA48010 from National Cancer Institute, NIH, and Department of Health and Human Services, National Science Foundation MCB RUI Grant 9057010 (to JAO, SSN, RAH); and NIH Grant CA39248 (to DB). 1. *Mol Cancer Ther*. 2002;1(8):617–28.
- Kraus M, Wolf B. Implications of acidic tumor microenvironment for neoplastic growth and cancer treatment: a computer analysis. *Tumor Biol*. 1996;17(3):133–54.
- Stock C. Schwab a protons make tumor cells move like clockwork. *Pflüg Arch Eur J Phy*. 2009;458(5):981–92.
- Stock C, Cardone RA, Busco G, Krähling H, Schwab A, Reshkin SJ. Protons extruded by NHE1: digestive or glue? *Eur J Cell Biol*. 2008;87(8-9):591–9.
- Švastová E, Hulíková A, Rafajová M, Zat'ovičová M, Gibadulinová A, Casini A, et al. Hypoxia activates the capacity of tumor-associated carbonic anhydrase IX to acidify extracellular pH. *FEBS Lett*. 2004;577(3):439–45.
- Zhang X, Ogorevc B, Wang J. Solid-state pH nanoelectrode based on polyaniline thin film electrodeposited onto ion-beam etched carbon fiber. *Anal Chim Acta*. 2002;452(1):1–10.
- Ke G, Zhu Z, Wang W, Zou Y, Guan Z, Jia S, et al. A cell-surface-anchored ratiometric fluorescent probe for extracellular pH sensing. *ACS Appl Mater Interfaces*. 2014;6(17):15329–34.
- Kenney RM, Boyce MW, Whitman NA, Kromhout BP, Lockett MR. A pH-sensing optode for mapping spatiotemporal gradients in 3D paper-based cell cultures. *Anal Chem*. 2018;90(3):2376–83.
- Pan T, Yang C, Li J, Jiang J, Wen J, Wang Z, et al. High-throughput extracellular pH monitoring and antibiotics screening by polymeric fluorescent sensor with LCST property. *Methods*. 2019;168:51–61.
- Zeng S, Liu D, Li C, Yu F, Fan L, Lei C, et al. Cell-surface-anchored ratiometric DNA tweezer for real-time monitoring of extracellular and apoptotic pH. *Anal Chem*. 2018;90(22):13459–66.
- Wang J, Geng Y, Shen Y, Shi W, Xu W, Xu S. SERS-active fiber tip for intracellular and extracellular pH sensing in living single cells. *Sens. Actuators. B: Chem*. 2019;290:527–34.
- Xu M, Ma X, Wei T, Lu Z-X, Ren B. In situ imaging of live-cell extracellular pH during cell apoptosis with surface-enhanced Raman spectroscopy. *Anal Chem*. 2018;90(23):13922–8.
- Pan C, Li X, Sun J, Li Z, Zhang L, Qian W, et al. A multiplexed SERS-active microneedle for simultaneous redox potential and pH measurements in rat joints. *ACS Applied Bio Mater*. 2019;2(5):2102–8.
- Sun F, Zhang P, Bai T, Galvan DD, Hung H-C, Zhou N, et al. Functionalized plasmonic nanostructure arrays for direct and accurate mapping extracellular pH of living cells in complex media using SERS. *Biosens Bioelectron*. 2015;73:202–7.
- Bi L, Wang Y, Yang Y, Li Y, Mo S, Zheng Q, et al. Highly sensitive and reproducible SERS sensor for biological pH detection based on a uniform gold nanorod array platform. *ACS Appl Mater Interfaces*. 2018;10(18):15381–7.

23. Sakata T, Sugimoto H, Saito A. Live monitoring of microenvironmental pH based on extracellular acidosis around cancer cells with cell-coupled gate ion-sensitive field-effect transistor. *Anal Chem.* 2018;90(21):12731–6.
24. Demoin DW, Wyatt LC, Edwards KJ, Abdel-Atti D, Sarparanta M, Pourat J, et al. PET imaging of extracellular pH in tumors with ⁶⁴Cu- and ¹⁸F-labeled pHLIP peptides: a structure–activity optimization study. *Bioconjug Chem.* 2016;27(9):2014–23.
25. García-Martín M-L, Hérigault G, Rémy C, Farion R, Ballesteros P, Coles JA, et al. Mapping extracellular pH in rat brain gliomas in vivo by H magnetic resonance spectroscopic imaging: comparison with maps of metabolites. *Cancer Res.* 2001;61(17):6524–31.
26. Provent P, Benito M, Hiba B, Farion R, López-Larrubia P, Ballesteros P, et al. Serial in vivo spectroscopic nuclear magnetic resonance imaging of lactate and extracellular pH in rat gliomas shows redistribution of protons away from sites of glycolysis. *Cancer Res.* 2007;67(16):7638–45.
27. Gyurcsányi RE, Pergel É, Nagy R, Kapui I, Thu Lan BT, Tóth K, et al. Direct evidence of ionic fluxes across ion-selective membranes: a scanning electrochemical microscopic and potentiometric study. *Anal Chem.* 2001;73(9):2104–11.
28. Kovács B, Csóka B, Nagy G, Kapui I, Gyurcsányi RE, Tóth K. Automatic target location strategy—a novel approach in scanning electrochemical microscopy. *Electroanalysis.* 1999;11(5):349–55.
29. Gyurcsányi RE, Nybäck A-S, Ivaska A, Tóth K, Nagy G. Novel polypyrrole based all-solid-state potassium-selective microelectrodes. *Analyst.* 1998;123(6):1339–44.
30. Joshi VS, Sheet PS, Cullin N, Kreth J, Koley D. Real-time metabolic interactions between two bacterial species using a carbon-based pH microsensor as a scanning electrochemical microscopy probe. *Anal Chem.* 2017;89(20):11044–52.
31. Zhu Z, Liu X, Ye Z, Zhang J, Cao F, Zhang J. A fabrication of iridium oxide film pH micro-sensor on Pt ultramicroelectrode and its application on in-situ pH distribution of 316L stainless steel corrosion at open circuit potential. *Sensor Actuat B-Chem.* 2018;255:1974–82.
32. Ratanapomcharoen C, Tabata M, Kitasako Y, Ikeda M, Goda T, Matsumoto A, et al. pH mapping on tooth surfaces for quantitative caries diagnosis using micro Ir/IrOx pH sensor. *Anal Chem.* 2018;90(7):4925–31.
33. Hampel M, Schenderlein M, Schary C, Dimper M, Ozcan O. Efficient detection of localized corrosion processes on stainless steel by means of scanning electrochemical microscopy (SECM) using a multi-electrode approach. *Electrochem Commun.* 2019;101:52–5.
34. Horrocks BR, Mirkin MV, Pierce DT, Bard AJ, Nagy G, Toth K. Scanning electrochemical microscopy. 19. Ion-selective potentiometric microscopy. *Anal Chem.* 1993;65(9):1213–24.
35. Liu Y, Liu H, Yao Z, Diao Y, Hu G, Zhang Q, et al. Fabrication, improved performance, and response mechanism of binary Ag–Sb alloy pH electrodes. *Electrochim Acta.* 2020. <https://doi.org/10.1016/j.electacta.2020.135746>.
36. Munteanu R-E, Stănică L, Gheorghiu M, Gáspár S. Measurement of the extracellular pH of adherently growing mammalian cells with high spatial resolution using a voltammetric pH microsensor. *Anal Chem.* 2018;90(11):6899–905.
37. Lee S-K, Boron WF, Parker MD. Monitoring ion activities in and around cells using ion-selective liquid-membrane microelectrodes. *Sensors.* 2013;13(1):984–1003.
38. Zając M, Lewenstam A, Stobiecka M, Dołowy K. New ISE-based apparatus for Na⁺, K⁺, Cl⁻, pH and Transepithelial potential difference real-time simultaneous measurements of ion transport across epithelial cells monolayer—advantages and pitfalls. *Sensors.* 2019;19(8):1881.
39. Zając M, Lewenstam A, Dołowy K. Multi-electrode system for measurement of transmembrane ion-fluxes through living epithelial cells. *Bioelectrochemistry.* 2017;117:65–73.
40. Bhandokar AJ, Hung VW, Jia W, Valdés-Ramírez G, Windmiller JR, Martinez AG, et al. Tattoo-based potentiometric ion-selective sensors for epidermal pH monitoring. *Analyst.* 2013;138(1):123–8.
41. Park HJ, Yoon JH, Lee KG, Choi BG. Potentiometric performance of flexible pH sensor based on polyaniline nanofiber arrays. *Nano Converg.* 2019;6(1):9.
42. Morris CA, Chen C-C, Ito T, Baker LA. Local pH measurement with scanning ion conductance microscopy. *J Electrochem Soc.* 2013;160(8):H430–5.
43. Chen CC, Chen YZ, Huang YJ, Sheu JT. Using silicon nanowire devices to detect adenosine triphosphate liberated from electrically stimulated HeLa cells. *Biosens. Bioelectron.* 2011;26(5):2323–8. <https://doi.org/10.1016/j.bios.2010.10.003>.
44. Bae JH, Brocenschi RF, Kisslinger K, Xin HL, Mirkin MV (2017) dissolution of Pt during oxygen reduction reaction produces Pt nanoparticles. *Anal Chem.* 2017;89(23):12618–21.
45. Zhang J, Kong L-B, Wang B, Luo Y-C, Kang L. In-situ electrochemical polymerization of multi-walled carbon nanotube/polyaniline composite films for electrochemical supercapacitors. *Synthetic Met.* 2009;159(3–4):260–6.
46. Buck RP, Lindner E. Recommendations for nomenclature of ionselective electrodes (IUPAC recommendations 1994). *Pure Appl Chem.* 1994;66(12):2527–36.
47. Qi G, Wang B, Zhang Y, Li H, Li C, Xu W, et al. Living-cell imaging of mitochondrial membrane potential oscillation and phenylalanine metabolism modulation during periodic Electrostimulation. *Anal Chem.* 2019;91(15):9571–9.
48. Grossman N, Bono D, Dedic N, Kodandaramaiah SB, Rudenko A, Suk H-J, et al. Noninvasive deep brain stimulation via temporally interfering electric fields. *Cell.* 2017;169(6):1029.e1016–41.e1016.
49. Li C, Xu S, Wang M, Jin Y. Smart plasmonic nanorobot for real-time monitoring cytochrome c release and cell acidification in apoptosis during electrostimulation. *Anal Chem.* 2018;91(2):1408–15.
50. Amemiya S, Guo J, Xiong H, Gross DA. Biological applications of scanning electrochemical microscopy: chemical imaging of single living cells and beyond. *Anal Bioanal Chem.* 2006;386(3):458–71. <https://doi.org/10.1007/s00216-006-0510-6>.

Publisher's note Springer Nature remains neutral with regard to jurisdictional claims in published maps and institutional affiliations.